Hybridisation of Non-Linear Behavioural Models with the TLM Full-Field Model

G. Kergonou, C. Christopoulos
GGIEMR, University of Nottingham
University Park, Nottingham, NG7 2RD, UK
Tel.: +44-(0)115-846-8296   Fax: +44-(0)115-951-5616
gaelle.kergonou@nottingham.ac.uk
christos.christopoulos@nottingham.ac.uk

F.G. Canavero
DELEN, Politecnico di Torino
Corso Duca degli Abruzzi, 24
10129 Torino, Italy
Tel.: +39-011-564-4060   Fax: +39-011-564-4099
flavio.canavero@polito.it

Abstract—**We describe the inclusion of parametric behavioral macromodels within the Transmission-Line Modelling (TLM) method. The macromodels reproduce the input/output port non-linear behavior of digital integrated circuit (IC). They are integrated in the 3D electromagnetic full-field code Minisolve either through a current source or conductance of the medium. The numerical results are compared to experimental data.**

Macromodels; TLM; non-linear actif circuit;

I.   INTRODUCTION

The challenge when designing a high-speed electronic system is to meet levels of ElectroMagnetic Compatibility (EMC) and Signal Integrity (SI). Interconnects, their geometry and terminations are key elements. The influence of terminations increases when dealing with nonlinear active circuits. Therefore an accurate analysis of the electromagnetic behaviour requires a full-wave solver including models of active components. TLM method offers a suitable environment for incorporating active models. Indeed it exploits the field-circuit equivalence and has the advantage, compared to the finite-difference time-domain method (FDTD), of calculating field components at the same time and at the same location. Embedding can be realised in two ways: either through a external link to a circuit solver such as SPICE [1], or by direct embedding as in [2]-[5], restricted to diodes, and [6] with digital IC macromodels. The first option gives access to a wide range of models via the SPICE libraries. On the negative side it slows the calculation speed as the TLM code calls SPICE at each time step. The second option avoids the slow speed problem. The connection of macromodels to the TLM mesh can be integrated at different positions and over several cells [1]. The purpose of this paper is to extend [6] by providing other embedding options according to the TLM formulation used under Minisolve [9]. The implemented macromodels consider in the first instance the input and outport ports without supply port.

The discussion is organized around three parts. Section II explains briefly the Mπlog software. Section III is dedicated to the TLM-macromodel interface. It describes the formulation used in Minisolve code and discusses the possibilities of linking the models. Section IV presents numerical and measurement results.

II.   MπLOG

Mπlog (Macromodeling via Parametric Identification of LOgic Gates) models the external port electrical characteristics of digital IC [8]. The macromodel generation needs knowledge of the voltage and current responses at the ports, obtained either from simulations or measurements. The models are based on a Local Linear State-Space (LLSS) parametric representation (1) and may also take into account the supply port.

$$x[k] \; = \; A \, x[k \text{-} 1] \; + \; B \, v[k \text{-} 1]. \qquad (1)$$

$$F_d(\theta; v[k]) \; = \; C \, x[k] \; + \; D \, v[k].$$

The relations (2) and (3) define in discrete time respectively the current of the input ports of receivers (2) -Fig. 1 left side- and output ports of drivers (3) -Fig. 1 right side - for single-ended configurations without supply port.

$$i_{rec}[k] \; = \; F_s(v[k]) \; + \; F_d(\theta; v[k]). \qquad (2)$$

$$i_{drv}[k] \; = \; w_H[k] \, i_H[k] \; + \; w_L[k] \, i_L[k]. \qquad (3)$$

where, k is the discrete time variable, $v[k]$ the voltage, $F_s(v[k])$ the static part and $F_d(\theta; v[k])$ the dynamic one described by the LLSS (1). w_H and w_L are switching signals accounting for the logic state evolution of the buffer. They are composed of concatenation of basic "up" and "down" signals computed during the model estimation process. Currents i_H and i_L (3) are expressed by a relation analogous to (2).
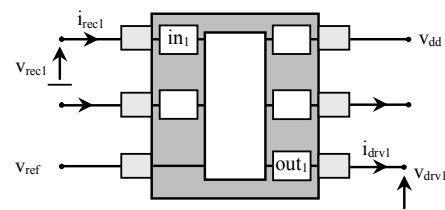

Figure 1. Input and output port models.
in$_1$ and out$_1$ are the input and output buffers.
V_{dd} and V_{ref} indicate the power supply voltages.

73

The created models are stable, compact (i.e fast), accurate and are readily integrated in any SPICE-like solvers or VHDL-AMS descriptions. Moreover, the data are also available in a Matlab workspace. This format is used to retrieve all the needed informations for the implementation of (1)-(3) in the full-wave solver.

III. TLM – MACROMODEL INTERFACE

This section deals with the parametric model interface within the TLM. First the TLM formulation used in Minisolve is described. Then possible ways to include the models are treated.

A. Minisolve

Minisolve includes the Z-transform TLM formulation developed in [9]. The computational domain is discretised in cubic unit cells based on the symmetrical condensed node (SCN) depicted in Fig. 2. The SCN is composed of twelve ports ($V_0 \ldots V_{11}$) and six field components (E_x, E_y, E_z, H_x, H_y, H_z) evaluated at the cell center. Equation (4) gives the expressions for equivalent (x,y,z) directed voltages and currents used in the scattering process for isotropic and nonmagnetic materials.

$$V_x = T_e (2V^r_x + \zeta^{-1} S_{ex}). \quad (4)$$

$$V_y = T_e (2V^r_y + \zeta^{-1} S_{ey}). \qquad V_z = T_e (2V^r_z + \zeta^{-1} S_{ez}).$$

$$i_x = T_m (-2 i^r_x + \zeta^{-1} S_{mx}).$$

$$i_y = T_m (-2 i^r_y + \zeta^{-1} S_{my}). \qquad i_z = T_m (-2 i^r_z + \zeta^{-1} S_{mz}).$$

with

$$2V^r_x = 2[V_0 + V_1 + V_2 + V_3]^i - i_{fx}. \quad (5)$$

$$2V^r_y = 2[V_4 + V_5 + V_6 + V_7]^i - i_{fy}.$$

$$2V^r_z = 2[V_8 + V_9 + V_{10} + V_{11}]^i - i_{fz}.$$

$$-2 i^r_x = -2[V_6 - V_7 - V_8 + V_9]^i - V_{fx}.$$

$$-2 i^r_y = -2[V_{10} - V_{11} - V_0 + V_1]^i - V_{fy}.$$

$$-2 i^r_z = -2[V_2 - V_3 - V_4 + V_5]^i - V_{fz}.$$

$$S_{ex} = 2V^r_x + \Gamma_e V_x - g_{ee}(\zeta) V_x + 4\chi_{ee}(\zeta) V_x. \quad (6)$$

$$S_{ey} = 2V^r_y + \Gamma_e V_y - g_{ee}(\zeta) V_y + 4\chi_{ee}(\zeta) V_y.$$

$$S_{ez} = 2V^r_z + \Gamma_e V_z - g_{ee}(\zeta) V_z + 4\chi_{ee}(\zeta) V_z.$$

$$S_{mx} = -2i^r_x + \Gamma_m i_x.$$

$$S_{my} = -2i^r_y + \Gamma_m i_y.$$
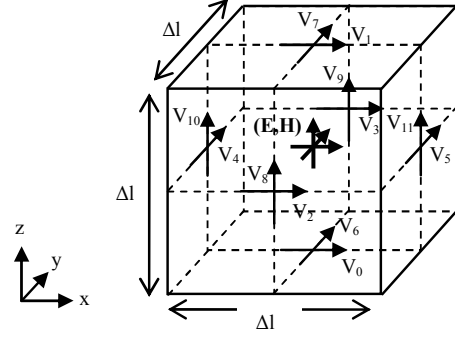
$$S_{mz} = -2i^r_z + \Gamma_m i_z.$$

Figure 2. 3D symmetrical condensed node

$$T_e = (4 + g_{e0} + 4\chi_{e0})^{-1}. \quad \Gamma_e = - (4 + g_{e1} - 4\chi_{e1}). \quad (7)$$

$$T_m = 1 / 4. \qquad\qquad \Gamma_m = - 4.$$

V^r, i^r denote the reflected fields (5), $[]^i$ the incident voltages, i_f and V_f respectively the free electric current and magnetic voltage, S the past events (6), T_e (T_m) and Γ_e (Γ_m) (7) respectively the transmission and reflection coefficients of the node. (g_{e0}, g_{e1}, $g_{ee}(\zeta)$) and (χ_{e0}, χ_{e1}, $\chi_{ee}(\zeta)$) components result of the partial fraction expansion of the electric conductance $g_e(\zeta)$ and susceptibility $\chi_e(\zeta)$ of the medium ((23), (24) in [9]).

[1][4] show that SPICE simulator can be coupled to the TLM mesh at three different places: node center, cell boundary, or halfway between them. As long as the circuit does not include resonant structures, the three approaches lead to good results [1].
(1)-(3) define the macromodel behaviour at the same time step. The current and voltage being unknowns, they need to be determined simultaneously. This restricts the implementation to the most natural one: at the node center, with different options that are discussed below. The node center embedding has the advantage of taking into account information coming from the four boundaries in relation with the model orientation, which is not the case for a boundary implementation.

B. Implementation hypothesis

Let's assume that the macromodel is z-oriented and spreads on one single cell. The voltage V_{macro} developed on the device corresponds to the voltage at the node center V_z, and, the current I_{macro} can be taken into account either through the current source I_{fz} or through the conductance.

1) Current source: i_{fz} is the current source I_{fz} normalized to the free-space impedance η_0 i.e. $i_{fz} = \eta_0 I_{fz}$ thus $i_{fz} = \eta_0 I_{macro}$. Incorporated in (5) this gives (8). All the other free-sources are cancelled.

$$2V^r_z = 2[V_8 + V_9 + V_{10} + V_{11}]^i - \eta_0 I_{macro}. \quad (8)$$

(8) is then introduced in V_z (4), i.e. V_{macro}, that is rewritten as:

$$2[V_8 + V_9 + V_{10} + V_{11}]^i + \zeta^{-1} S_{ez} - \eta_0 I_{macro} - V_{macro}/T_e \leq \varepsilon. \quad (9)$$

to look for the pair (V_{macro}, I_{macro}) which meets the requested accuracy ε. The search is carried out with the modified multivariate secant method [10], knowing the incident voltages on the cell boundary and the past events (6). Once (V_{macro}, I_{macro}) are found, the information is scattered on the adjacent cells at the next time step by:

$$V^r_0 = V^r_x - i_y - V^i_1. \qquad V^r_1 = V_x + i_y - V^i_0. \qquad (10)$$

$$V^r_2 = V_x + i_z - V^i_3. \qquad V^r_3 = V_x - i_z - V^i_2.$$

$$V^r_4 = V_y - i_z - V^i_5. \qquad V^r_5 = V_y + i_z - V^i_4.$$

$$V^r_6 = V_y + i_x - V^i_7. \qquad V^r_7 = V_y - i_x - V^i_6.$$

$$V^r_8 = V_{macro} - i_x - V^i_9. \qquad V^r_9 = V_{macro} + i_x - V^i_8.$$

$$V^r_{10} = V_{macro} + i_y - V^i_{11}. \qquad V^r_{11} = V_{macro} - i_y - V^i_{10}.$$

In practical applications most part of ICs are surface mounted. The dielectric properties at the levels of input and output ports remain thus uniform. The implementation via current source maintains the uniformity of the medium.

2) Conductance: The device inclusion can be made through the conductance of the medium $g_e(\zeta)$. In that case, the conductance is no longer uniform in (x, y, z) and it becomes a tensor. Equations (4)-(7) apply only for isotropic or anisotropic without coupling. Thus $g_e(\zeta) = \text{diag}(g_{ex}(\zeta), g_{ey}(\zeta), g_{ez}(\zeta))$. The components $g_{ex}(\zeta)$, $g_{ey}(\zeta)$, that are identicals, can be fixed in two ways: either they conserve the medium losses (11) defined in the adjacent cells, or they are cancelled (12). The last option would further correspond to the implementation of a lumped element.

$$T_e = (4 + g_{ex0} + 4\chi_{ex0})^{-1}. \quad \Gamma_e = -(4 + g_{ex1} - 4\chi_{ex1}). \ (11)$$

$$S_{ex} = 2V^r_x + \Gamma_e V_x - g_{eex}(\zeta) V_x + 4\chi_{eex}(\zeta) V_x.$$

$$S_{ey} = 2V^r_y + \Gamma_e V_y - g_{eex}(\zeta) V_y + 4\chi_{eex}(\zeta) V_y.$$

where (g_{ex0}, g_{ex1}, $g_{eex}(\zeta)$) and (χ_{ex0}, χ_{ex1}, $\chi_{eex}(\zeta)$) are the coefficient of the partial fraction expansions in relation with the medium properties. V^r expressions (5) are modified such as all the free-sources are null. The current expressions have not been reported as unchanged.

$$T_e = (4 + 4\chi_{ex0})^{-1}. \qquad \Gamma_e = -4. \qquad (12)$$

$$S_{ex} = 2V^r_x + \Gamma_e V_x. \qquad S_{ey} = 2V^r_y + \Gamma_e V_y.$$

T_e and Γ_e in (12) correspond to the reflection and transmission coefficients of the free-space node.

Concerning component $g_{ez}(\zeta)$, it is simplified in g_{e0}:

$$g_{e0} = \eta_0 I_{macro}/V_{macro}. \qquad (13)$$

Indeed the macromodel is treated as a black-box within the mesh. That means $g_{ez}(\zeta)$ is independent of the previous events

i.e. $g_{e1} = 0$ and $g_{ee}(\zeta) = 0$. This leads to:

$$T_{ez} = (4 + g_{e0} + 4\chi_{e0})^{-1}. \qquad \Gamma_{ez} = -4. \qquad (14)$$

$$S_{ez} = 2V^r_z + \Gamma_{ez} V_z. \qquad V_z = T_{ez} (2V^r_z + \zeta^{-1} S_{ez}).$$

V_z (14) is rewritten as (15) by inserting (13) in T_{ez} (14) and S_{ez} as (16) after developing again the initial formulation of V_z (see (22) in [9]).

$$V_z = T_e (2V^r_z - \eta_0 I_{macro} + \zeta^{-1} S_{ez}). \qquad (15)$$

$$S_{ez} = 2V^r_z + \Gamma_{ez} V_z - \eta_0 I_{macro}. \qquad (16)$$

where T_e is defined as in (12). Hence the properties in the device orientation correspond to the free-space ones. It follows that implementing through the conductance enables an inclusion either in a free-space node ((15)(16)+(12)) or in a joint node ((15)(16)+(11)).

Equations (15)(16) apply to the input ports of receivers according to the sign conventions in Fig. 1. They are modified by $+ \eta_0 I_{macro}$ for the output ports of driver.

IV. EXPERIMENTAL VALIDATION

A PCB has been made to validate the hybridization. This section presents the measurements and the numerical results.

A. Printed Circuit Board

Fig. 3 shows the test board. It consists of a driver (left side) and a receiver (right side) linked with a microstrip line. The strip is 800 μm wide, 100 mm long. The substrate is 400 μm thick with a relative permittivity $\varepsilon_r = 4.24$ and dielectric losses of 0.01 at 1 MHz. In theory [11][12] the characteristic impedance is $Z_c \approx 49.5 \ \Omega$ and the effective permittivity $\varepsilon_{re} \approx 3.23$ (average at the frequencies of interest) either a propagation time $T_d \approx 0.6$ ns for L = 100 mm.
The ICs are the SN74AHC1G04-Q1 single inverter from Texas Instruments (TI). They are supplied with ($V_{DD} = 4.8$ V; $V_{ref} = 0$ V).

The transient waveforms are collected with the LeCroy WavePro 7300A scope (3 GHz bandwidth, 10 GS/s) and the P6158 passive voltage probe (3 GHz bandwidth, 1 kΩ, 1.5 pF, 20x attenuation, 5ns delay). Fig. 4 reports the output (V_{drv}) and input (V_{rec}) port voltages got for the input voltage V_{in}: $V_M = V_{DD}$, $t_r = t_f = 10$ ns, delay = 13.9 ns, $W_{high} = 42.1$ ns, T = 100 ns.
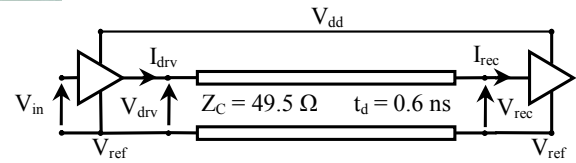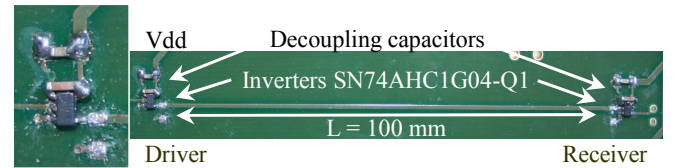

Figure 3. Test board

B. TLM structure

Fig. 5 shows the modelled structure in the TLM code. The dimensions are specified with the discretisation step dl = 400 μm, that corresponds to a time step $\Delta t = 0.67$ ps. The strip is zero-thickness and perfectly conducting, the substrate is assumed lossless. The configuration is surrounded by matched boundary conditions in the lateral and top directions and a perfect electric conductor one at the substrate back. The full-wave simulation carried out with a gaussian voltage source indicates a transmission line with $Z_c \approx 51\ \Omega$ and $T_d \approx 0.67$ ns.

The strip is fed by the driver that the switching signals (2) are built from the measured voltage V_{in}. It is loaded by the receiver. The macromodels are generated with the SN74AHC1GU04 HSPICE model, under the power supply: $V_{DD} = 4.8$ V; $V_{ref} = 0$ V. According to TI, this model applies to the SN74AHC1G04-Q1. The models are established with the sampling time $T_s = 50$ ps and resampled to the TLM time step.

Fig. 4 presents the full-wave simulation results. A good agreement is observed. Note a difference at the transition end linked to the time delay of the probe (5 ns) that affects the signal measurements with fast switching time (around 3 ns here).
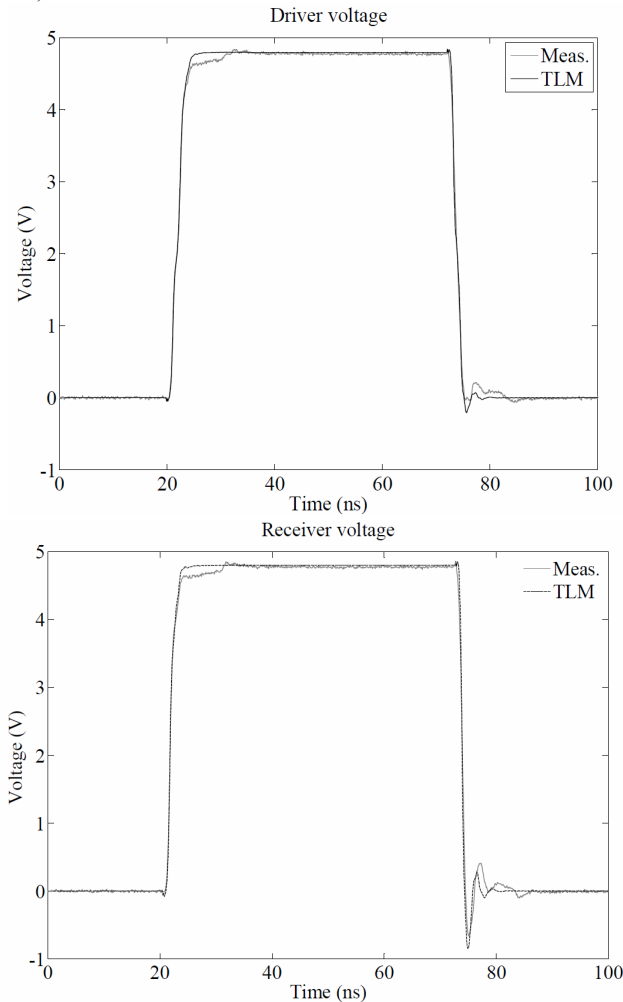

Figure 5. Microstrip structure used for the hybridization validation

Figure 4. Comparison of driver (top) and receiver (bottom) voltages got by measurements and simulations with HPSICE and TLM

V. CONCLUSION

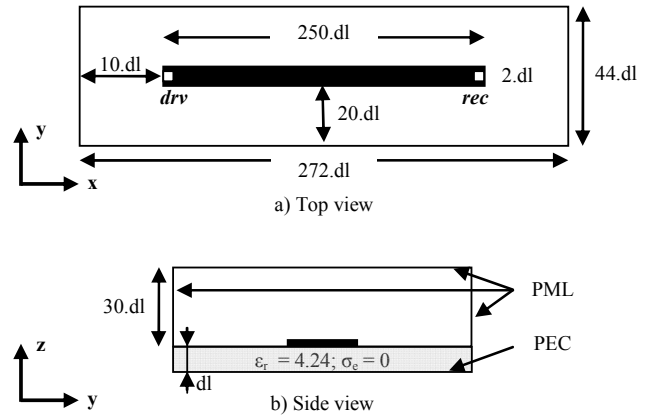Models reproducing the I/O port non-linear behavior of an IC have been implemented in a full-wave TLM solver. Different connections within one single cell have been discussed. The comparison of numerical and experimental results have validated the hybridisation.

REFERENCES

[1] P.P.M. So, W.J.R. Hoefer, "A TLM-SPICE Interconnection framework for coupled field and circuit analysis in the time domain", IEEE Trans. on MTT, vol. 50, no 12, pp 2728-2733, December 2002.

[2] P. Russer, P.P.M. So, W. J. R. Hoefer , "Modeling of nonlinear active regions in TLM", IEEE Microwave and guided wave letters, vol. 1, no 1, pp 10-13, January 1991.

[3] L. Cascio, G. Tardioli, W.J.R. Hoefer, "Modeling of nonlinear active and passive devices in three dimensional TLM networks", IEEE MTT-S, pp 383-386, 1997.

[4] J.W. Park, P.P.M. So, W.J.R. Hoefer, "Lumped and distributed device embedding techniques in time domain TLM field models", IEEE MTT-S, pp 2047-2050, May 2001.

[5] M.I. Sobhy, E.A. Hosny, P. Russer, B. Isele, C. Christopoulos, "Interfacing the transmission line method (TLM) and state-space (SS) techniques to analyse general non-linear structures", Computation in Electromagnetics conf., pp 299-302, 1994.

[6] G. Kergonou, F.G. Canavero, "Implémentation de modèles de circuits non-linéaires sous la TLM", CEM 2010 Limoges.

[7] Minisolve code, GGIEMR University of Nottingham.

[8] I.S. Stievano, C. Siviero, F.G. Canavero, I.A. Maio, "Behavioral modeling of digital devices via composite Local-linear State-space relations", IEEE Trans. on Instrumentation and Measurement, vol. 57, no 8, pp 1757-1765, August 2008.

[9] J. Paul, C. Christopoulos, D.W.P. Thomas, "Generalized material models in TLM-Part I: materials with frequency-dependent properties", IEEE trans. on AP, vol. 47, no 10, pp 1528-1534, October 1999.

[10] M. Podisuk, "Modified multivariate secant method", Universitatis Iagellonicae Acta Mathematica, Fasciculus XXI, pp 265-267, 1994.

[11] E. Hammerstad and O. Jensen, "Accurate models for microstrip computer aided design", IEEE MTT-S, pp 407-409, 1980.

[12] M. Kirschning and R.H. Jansen, "Accurate model for effective dielectric constant of microstrip with validity up to millimeter-wave frequencies", Electronics letters, vol. 18, no 6, pp 272-273, March 1982.